International Journal of Scientific Research in Engineering and Management (IJSREM)
Volume: 09 Issue: 12 | Dec - 2025 SJIF Rating: 8.586 ISSN: 2582-3930

Influence of Nd^{3+} Doping on the Structural Infrared and IV Characteristic of Nickel Ferrite

Sagar Rathod[1*] Vikas Magar[1], Smita More[2], D. R. Sapate[3]
[*1]Department of Physics, Deogiri College, Chhatrapati Sambhajinagar-431001, (MS), India
[2]Dept. of Basic Sciences and Humanities, Maharashtra Institute of Technology, Chhatrapati Sambhajinagar-431010, (MS), India
[3]Department of Physics, Sant Ramdas Arts, Commerce, and Science College, Ghansawangi, Jalna-431209, (MS), India

Abstract
In this study, nanocrystalline thin films of Nd^{3+}doped spinel ferrite, represented by the chemical formula $NiFe_{2-x}Nd_xO_4$ (where x = 0.00, 0.02, and 0.04), were successfully synthesized using the spray pyrolysis deposition technique. The films were deposited onto glass substrates that had been thoroughly cleaned using ultrasonic treatment. X-ray diffraction (XRD) analysis confirmed the formation of a single-phase cubic spinel structure, with characteristic peaks observed at (220), (311), (222), (400), (422), (511), and (540). The absence of secondary phases in the XRD patterns supports the phase purity of the deposited films. Crystallite sizes, calculated using the Debye-Scherrer equation, were found to range between 15 nm and 9 nm. A systematic decrease in lattice parameters was observed with increasing Nd^{3+} doping, indicating successful substitution at the iron sites. Fourier-transform infrared (FTIR) spectroscopy revealed distinct absorption bands around 400 cm^{-1} and 600 cm^{-1}, corresponding to metal–oxygen stretching vibrations within the spinel lattice. Current–voltage (I–V) measurements confirmed the ohmic behaviour of the thin films, suggesting their potential applicability in electronic devices.
Keywords: Spray deposition, Thin Films, XRD, FTIR, I-V

1. Introduction

Oxide magnetic materials, such as ferrites, are commonly used by a number of researchers to investigate various properties for different applications [1]. The combination of electrical and magnetic properties associated with ferrite is of great interest to many researchers [2]. They exhibit high electrical resistivity, high saturation magnetization, low eddy-current and dielectric losses, high magneto-crestline anisotropy, and high permeability [3]. etc., which are a useful number of applications [4]. On the basis of combine electrical and magnetic properties ferrite have application in the field of transformer cover antimatroid, high frequency devices, sensors, catalyst etc [5] recently nanoparticles of ferrite have gained lot of importance because of their smaller size of the order of Nano dimension, large surface to volume ratio from greater stability, by biocompatible, less toxic, [6] easy to synthesis etc many researcher have investigated the structural morphological optical magnetic an another properties of ferrite Nano particle ferrite crestline in three groups namely spinel ferrite rare earth garnet and hexagonal ferrite [7].

Among this class of ferrites, spinel ferrite is largely studied by a number of researchers [8]. The spinel ferrite in thin films exhibits enhanced surface area and a range of applications [9]. The thin film of spinel ferrite is prepared by physical methods and chemical methods [10]. The physical method includes plus

deposition method, scattering, etc, the chemical method includes spray pyrolysis, chemical bath deposition, chemical vapour deposition, etc [11, 12]. Among these methods, spray pyrolysis is one of the best methods for fabricating the thin films of spinel ferrite [13, 14]. The Nano crestline thin film can be prepared by the sol-gel method, which can be deposited on a clean glass substrate [15]. The spinel ferrites are represented by the formula MFe_2O_4, where M can be a metal, such as iron, cobalt, nickel, zinc, cadmium, magnesium, etc [16]. The crystal structure of spinel ferrite has two industrial sites: the tetrahedral A and octahedral B sites [17]. Nickel ferrite is one of the important spinel ferrites, exhibiting both electrical and magnetic properties for desired applications [18]. The properties of nickel ferrite thin films can be varied by doping with types of divalent, trivalent, and tetravalent cations [19]. Rare-earth iron doped in nickel ferrite can also exhibit these properties. In the literature, Nd doped Nickel Ferrite thin films deposited by the spray pyrolysis technique have not been reported to the best of our knowledge [20]. Hence, an attempt is made to prepare Nd doped nickel ferrite ($NiFe_{2-x}Nd_xO_4$, x = 0.00,0.02,0.04) thin films using the spray pyrolysis technique. The structural, Fourier transform infrared spectroscopy, and I-V characteristics are reported in this work [21].

2. Experimental Technique

2.1. Materials and Methods:

AR grade nickel nitrate hexahydrate ($Ni(NO_3)_2.6H_2O$), neodymium nitrate hexahydrate ($Nd(NO_3)_3 \cdot 6H_2O$), and ferric nitrate nonahydrate ($Fe(NO_3)_3.9H_2O$) were used as starting materials. The glass substrates were carefully dipped in chromic acid for 45 min. This glass substrate was cleaned in the ultrasonic bath for 25-30 min and used for the deposition of the film.

Table. 1: Refined parameters for the spray deposition of $NiFe_{2-x}Nd_xO_4$ (x = 0.00, 0.02, and 0.04)

Parameters	Specification
Molarity proportion	1:2
Volume proportion	1:2
Substrate type and dimensions: Cleaned glass	(75 mm × 25 mm × 1.35 mm)
Nozzle to substrate distance	29cm
Spray rate	2-6 ml/min
Spray pressure	0.25 Pa
Substrate temperature	380°C
Annealing temperature and time	500°C for three h

2.2. Synthesis

Thin films of $NiFe_{2-x}Nd_xO_4$ (x = 0.00, 0.02, and 0.04) were deposited on optically transparent glass substrates of dimensions 75 mm × 25 mm × 1.35 mm by employing the spray pyrolysis method. High-purity precursor salts (~99.98%), namely AR-grade nickel nitrate hexahydrate (Ni $(NO_3)_3 \cdot 6H_2O$), neodymium nitrate hexahydrate (Nd $(NO_3)_3 \cdot 6H_2O$), and ferric nitrate nonahydrate (Fe $(NO_3)_3 \cdot 9H_2O$), served as starting materials. Each nitrate compound was first dissolved individually in deionised water to prepare 0.1 M solutions of Ni^{2+}, Gd^{3+}, and Fe^{3+} ions. These solutions were then combined in such a manner that the cationic proportion of Ni^{2+} (Fe^{3+}+ Gd^{3+}) remained 1:2, in accordance with the stoichiometry of $NiFe_{2-x}Nd_xO_4$. Nickel nitrate provided the primary cationic source, while ferric nitrate, along with controlled quantities of aluminium and gadolinium nitrates, constituted the secondary fraction, thereby ensuring the required chemical composition of the final spray solution. The homogeneous precursor solution was atomised through a spray nozzle and directed onto glass substrates maintained at ~385 °C. The spraying pressure was maintained at approximately 0.26 Pa to ensure uniform film growth. Following each spray burst, the substrate temperature showed a slight decrease and typically required 2-4 minutes to return to the present value, which was regulated by a digital temperature controller. Other deposition parameters, including spray rate, pressure, and nozzle-to-substrate distance, were optimised and are presented in Table 1. After the deposition process, the substrates were kept at the same temperature for 20–30 minutes to ensure proper film formation and then allowed to cool gradually to room temperature. To improve crystallinity and remove any residual moisture or unwanted phases, the as-prepared films were annealed at 500 °C for 4 hours**. Figure 1** shows the Schematic diagram of the thin film deposition process on the glass substrate.

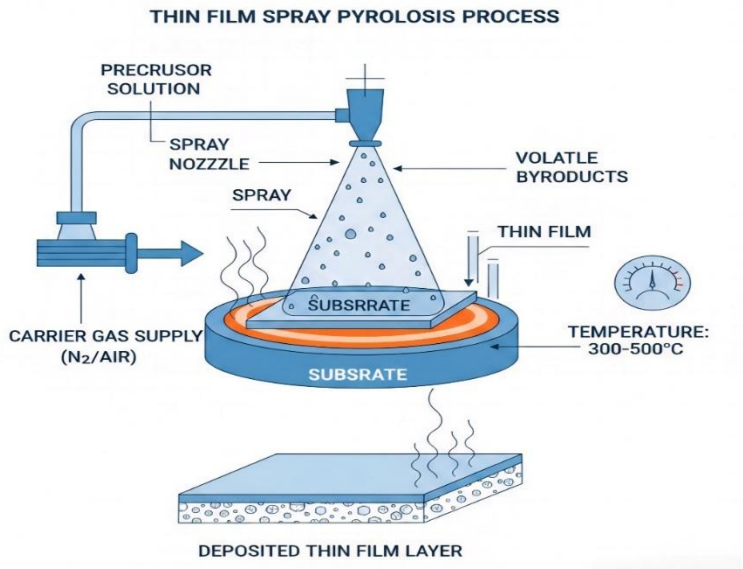

Figure 1. Schematic diagram of the thin film deposition process on the glass substrate.

2.3. Characterizations

To observe the structural, vibrational, and electrical characteristics of the Nd^{3+} substituted nickel ferrite thin films, a variety of analytical techniques were used. Structural analysis was performed using a BRUKER D8 Advance X-ray diffractometer with Cu-Kα radiation, within the 2θ scanning range of 20°–80°. The vibrational modes of the films were studied using Fourier Transform Infrared Spectroscopy (FTIR) using a JASCO FT-IR 6600 spectrophotometer, layer a spectral window from 4000 to 400 cm^{-1}. Raman scattering measurements were performed at room temperature with the STR-500 Micro-Raman spectrometer (Japan). Film thickness for the doped samples was projected using the width difference method.

3. Results and Discussion

3.1. Thin Film Thickness

The thickness of the prepared Nd^{3+} doped nickel ferrite thin films ($NiFe_{2-x}Nd_xO_4$, x=0.00,0.02,0.04) was measured by using the gravimetric weight difference method. A sensitive microbalance having an accuracy of 0.001 mg was used. The weight of the glass substrate before and after thin-film deposition was measured using a microbalance. The values of the thickness of the prepared thin films were estimated by employing the following relation (Eq.1).

$$t = \frac{\delta_m}{A\rho} \quad (1)$$

where t is the thickness of the thin film, δ_m is the mass difference, ρ is the density of the film, and A is the area of the thin film. The values of the thickness for various Nd^{3+} compositions are given in **Table 2.**

3.2. X-ray diffraction

Figure 2 depicts X-ray diffraction patterns of ($NiFe_{2-x}Nd_xO_4$, x = 0.00, 0.02, 0.04) spinel ferrite thin films deposited on a clean glass substrate using an optimized spray pyrolysis technique. Figure 1 reflects the orientation of diffraction peaks at different Bragg angles. All these diffraction pics are assigned Miller indices using Bragg's law and X-ray diffraction. The Pattern shows diffraction pics (220, 311, 222, 400, 422, 511, and 440). No peaks other than these diffraction peaks are observed in the X-ray pattern, consistent with the formation of a single-phase cubic structure in the films. The diffraction peak is intense and slightly broadened, which shows the nano-crestline nature of the film. The crystallite size was calculated using the Scherrer equation, and the values are given in the table. The structural parameters, such as lattice constant, unit cell volume, and X-ray density, were calculated using standard relations, and their values are also listed in **Table 1**. It is noted from **Table 1** that the lattice constant increased on doping Nd^{3+} ions. This can be attributed to the fact that larger Nd^{3+} ions (1.15 Å) replace smaller Fe^{3+} ions (0.67 Å). **Figure 3** shows the Variation of crystallite size and lattice constant with composition (x). This result shows an increasing lattice constant. Like lattice constant, unit cell volume, and ionic radii, the setting both increase with Nd^{3+} doping. The other structural parameters, such as stacking fault lattice strain, dislocation density, and macrostrain, were calculated using the following relations,

$$D = \frac{K\lambda}{\beta COS\theta}\ nm \quad (2)$$

$$\frac{1}{d^2} = \frac{h^2}{a^2} + \frac{k^2}{b^2} + \frac{l^2}{c^2}\ \text{Å} \quad (3)$$

The values of these microstructural parameters are listed in **Table 2.** It is observed that the lattice strain, macrostrain, and dislocation density increase with increasing Nd doping. The stacking fault was found to

be constant. Various microstructural parameters such as micro strain (ε), dislocation density (δ), stacking fault (SF), and lattice strain (LS) were calculated using the following relation (Eq. 4-6)

$$\varepsilon = \frac{\beta cos\theta}{4} \quad (4)$$

$$\delta = \frac{1}{D^2} \quad (5)$$

$$SF = \frac{2\pi^2}{45\sqrt{3}tan\theta} \quad (6)$$

$$LS = \frac{\beta}{4tan\theta} \quad (7)$$

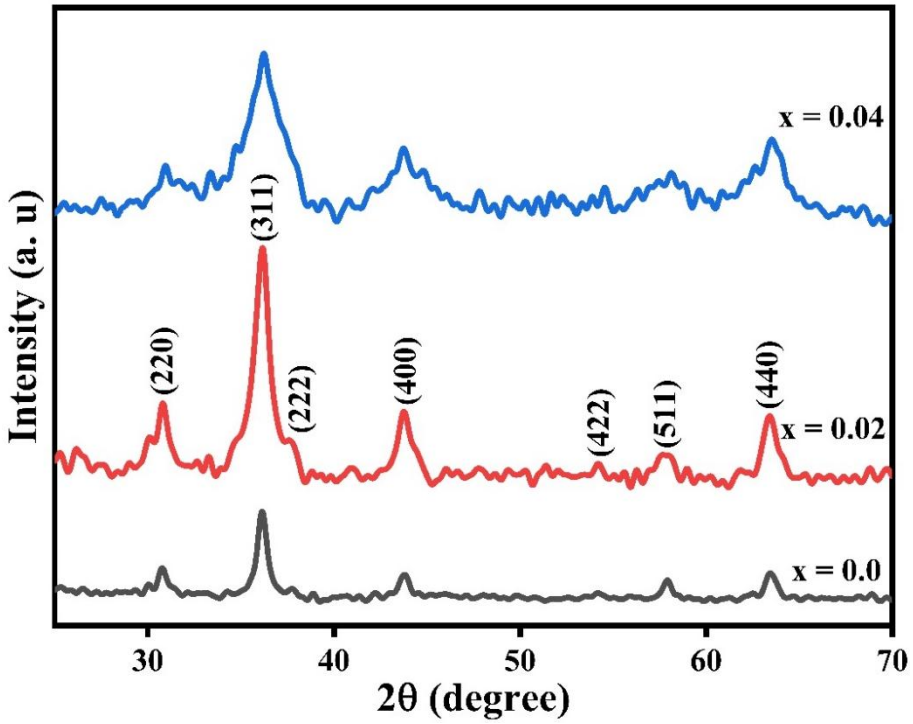

Figure 2. XRD patterns of $NiFe_{2-x}NdxO_4$ (x = 0.00, 0.02, and 0.04) thin films.

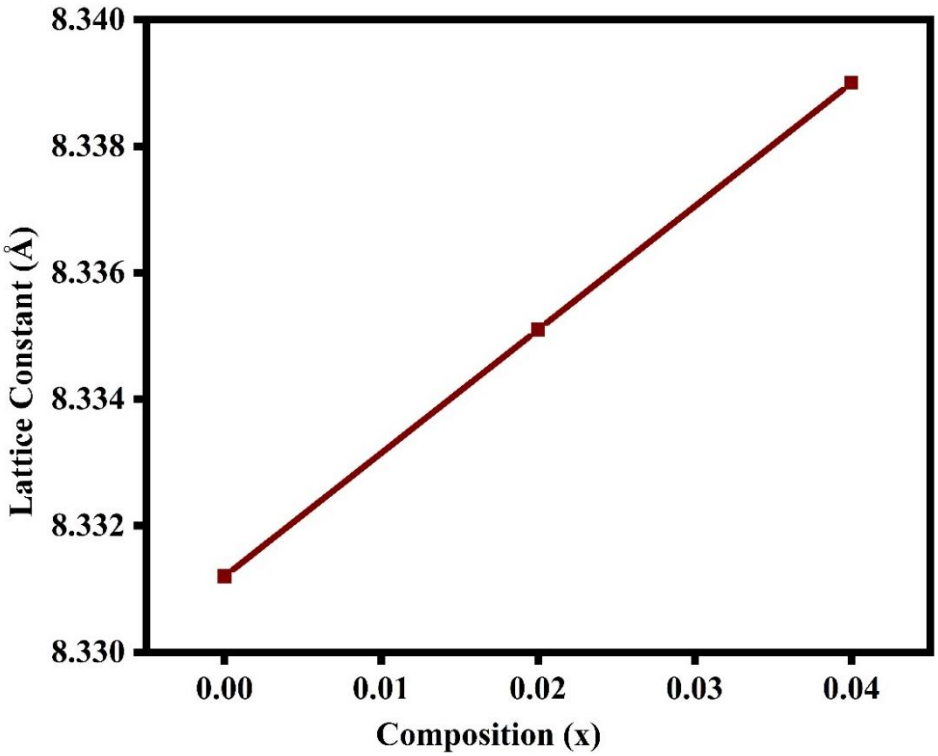

Figure 3. Variation of crystallite size and lattice constant with composition (x) of $NiFe_{2-x}O_4$ (x = 0.00,0.02 and 0.04) thin films.

Table .2: Measurements of $NiFe_{2-x}Nd_xO_4$ (x = 0.00, 0.02, and 0.04) thin films, including Thickness (t) in millimetres, Crystallite size (D) in nanometres, lattice Constant (a) in Angstroms, X-ray density (dx) in grams per cubic centimetre, and Volume in cubic Angstroms.

x	T (nm) ±5nm	D (nm)	a (Å) ±0.001Å	d_x (g/cc)
0.00	238	15	8.3312	5.3900
0.02	221	11	8.3351	5.5169
0.04	252	9	8.3390	5.6434

Table. 3: Values of Lattice strain (LS), macrostrain (ε), Dislocation density (δ), and Stacking fault (SF) for XRD patterns of $NiFe_{2-x}Nd_xO_4$ (x = 0.00, 0.02, and 0.04) thin films.

x	LS	ε	δ lines/m²	SF
0.00	0.0079	0.0023	0.0044	0.4278
0.02	0.0109	0.0032	0.0082	0.4284
0.04	0.0123	0.0037	0.0123	0.4288

3.3. Fourier Transform Infrared Spectroscopy

Figure 4 represents the Fourier Transform Infrared Spectra of Nd doped nickel ferrite thin films, which were recorded at room temperature. The spectra show two absorption bands close to 600 cm^{-1} and 400 cm^{-1}. These absorption bands are designated as υ_1 and υ_2, respectively. The values of υ1 and υ2 are given in Table 3. The υ_1 band is due to the intense vibration of the metal oxygen band at the tetrahedral site. The υ_2 band is due to the intense vibration of the metal oxygen band at the octahedral site. We observed that the difference in absorption bands may be due to differences in metal-oxygen bonds in tetrahedral (A) and octahedral [B]. Using the values of the absorption band, the force constant corresponding to the tetrahedral and octahedral was calculated using the following relation.

$$K_t = 7.62 \times M_A \times \nu_1^2 \times 10^{-7} \quad (8)$$

$$K_0 = 5.31 \times M_B \times \nu_2^2 \times 10^{-7} \quad (9)$$

$$K_{avg} = \frac{K_t \times K_0}{2} \quad (10)$$

The tetrahedral mass (M_A) and octahedral mass (M_B) were calculated by showing the following cation distribution.

(Fe) {Ni $Nd_xFe_{1-x}O_4$} (X = 0.00, 0.02, 0.04).

Nickel ferrite is an inverse spinel ferrite in which the enhanced or occupied octahedral [B] side and Fe^{3+} ions are distributed equally on both the tetrahedral (A) and octahedral [B] sites. Nd^{3+} ions are larger; hence, they occupy the octahedral [B] site. The values of force constant K_t and K_0 are presented in **Table 4.**

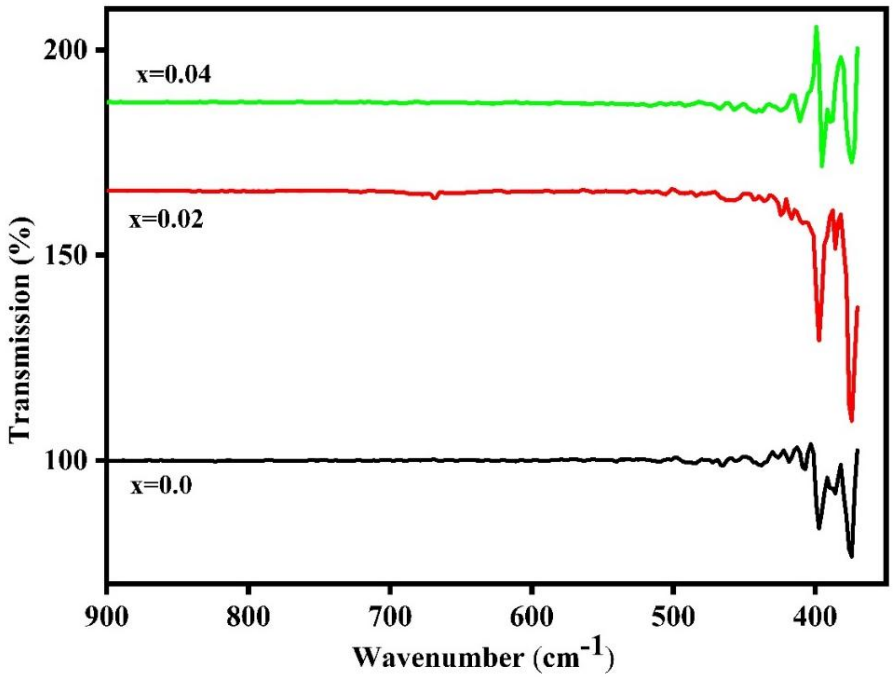

Figure 4. FTIR spectra of $NiFe_{2-x}Nd_xO_4$ (x = 0.00, 0.02, and 0.04) thin films

Table 4. Value of wavenumber at tetrahedral site (υ_1), wavenumber at octahedral site (υ_2) Force constant for tetrahedral site (K_t), force constant for octahedral site (K_o) and Average of force constant (K_{avg}) in FT-IR spectra of $NiFe_{2-x}Nd_xO_4$ (x = 0.00, 0.02, and 0.04) thin films

x	υ_1 (cm^{-1})	υ_2 (cm^{-1})	K_t ($*10^2$) N/m	K_0 ($*10^2$) N/m	K_{avg} ($*10^2$) N/m
0.00	574	396	1.40	9.53	1.17
0.02	582	397	1.44	9.73	1.20
0.04	586	394	1.46	9.73	1.21

3.4. Current- Voltage (I-V) Characterisation

Figures 4, 5, and 6 represent the current voltage characteristic of Nd^{3+} doped nickel ferrite. The I-V plot shows linear behaviour representing an ohmic nature. Using the I-V curve, the resistivity of nickel ferrite (x = 0.00) is found to be of the order of 1.1695. With Nd doping, resistivity is found to increase to 7.2163 and 9.1693, respectively, for (x = 0.02 and 0.04).

$$\rho = \frac{RA}{t} \quad (11)$$

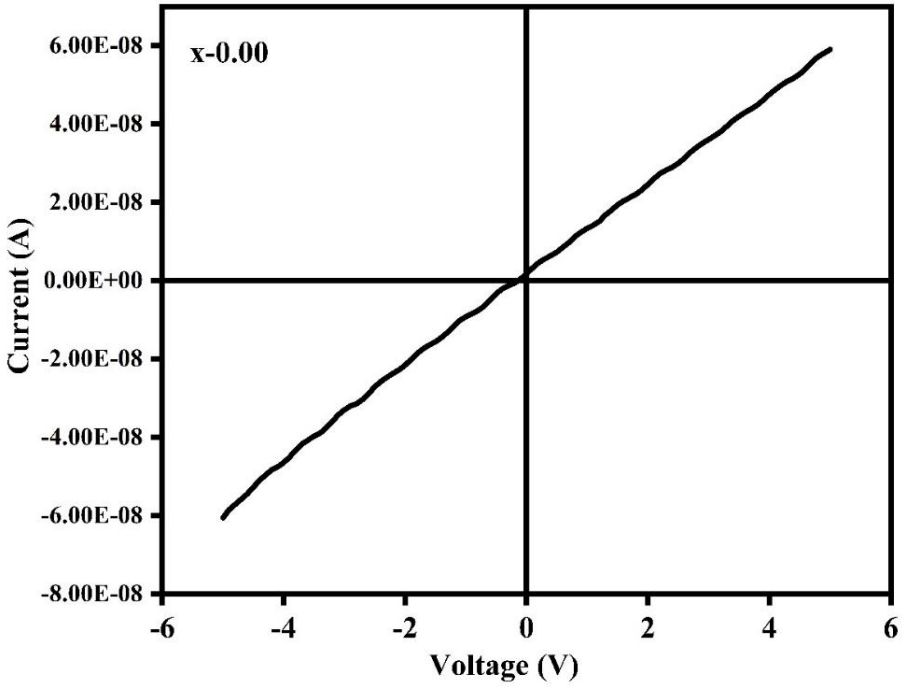

Figure 5. I-V curves of $NiFe_{2-x}NdxO_4$ (x = 0.00) thin films

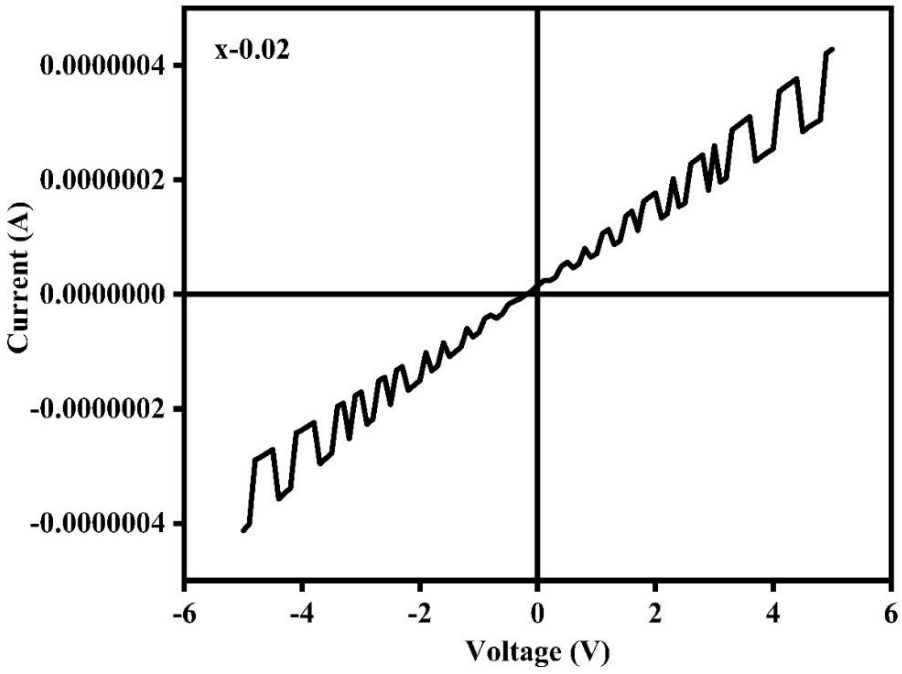

Figure 6. I-V curves of $NiFe_{2-x}NdxO_4$ (x = 0.02) thin films

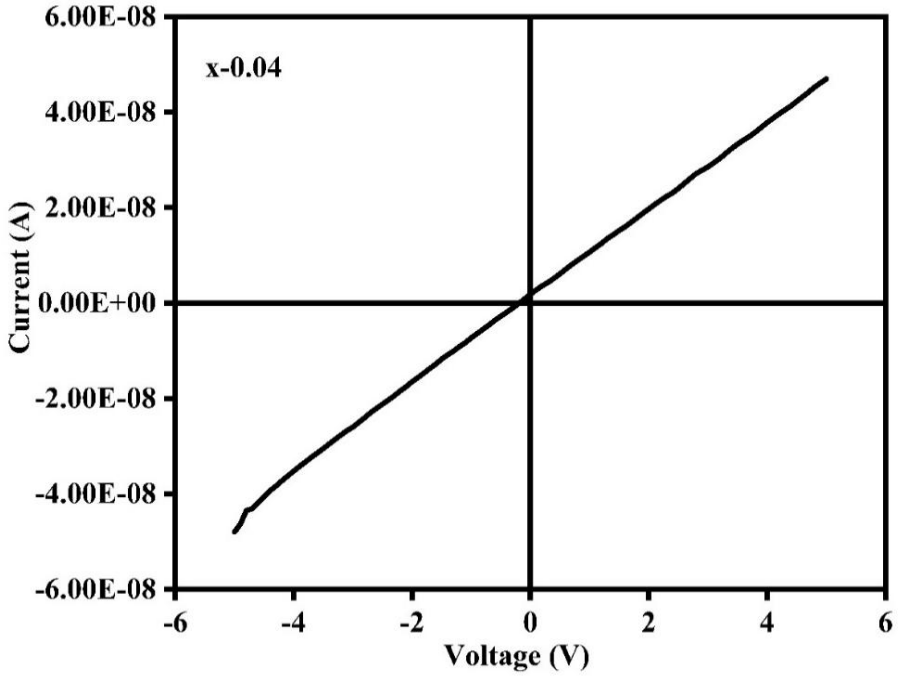

Figure 7. I-V curves of $NiFe_{2-x}NdxO_4$ (x = 0.04) thin films

Table. 5: Resistivity of $NiFe_{2-x}Nd_xO_4$ (x = 0.00, 0.02, and 0.04) thin films

X	0.00	0.02	0.04
Resistivity (Ω.m)	1.1695	7.2163	9.1693

4. Conclusions

Thus, spinel ferrite thin films of $NiFe_{2-x}Nd_xO_4$ (x=0.00,0.002,0.004) were successfully deposited uniformly on glass substrate using the spray pyrolysis technique. Single-phase production of the thin film was verified using X-ray diffraction analysis. The values of crystallite size suggest the nanocrystalline nature of the films. The structural, infrared, and I-V characteristics or influenced by Nd^{3+} doping. The lattice constant, force constant, and resistivity increase with increasing Nd^{3+} doping level.

Reference

1. Srivastava, R. and B.C. Yadav, *Ferrite materials: introduction, synthesis techniques, and applications as sensors.* International Journal of Green Nanotechnology, 2012. **4**(2): p. 141-154.
2. Pradeep, A., P. Priyadharsini, and G. Chandrasekaran, *Structural, magnetic and electrical properties of nanocrystalline zinc ferrite.* Journal of Alloys and Compounds, 2011. **509**(9): p. 3917-3923.
3. Zhang, Y., et al., *High-entropy alloys with high saturation magnetization, electrical resistivity, and malleability.* Scientific Reports, 2013. **3**(1): p. 1455.
4. Wang, F., et al., *Excellent soft magnetic Fe-Co-B-based amorphous alloys with extremely high saturation magnetization above 1.85 T and low coercivity below 3 A/m.* Journal of Alloys and Compounds, 2017. **711**: p. 132-142.
5. Kiran, M.R., et al., *A Comprehensive Review of Advanced Core Materials-Based High-Frequency Magnetic Links Used in Emerging Power Converter Applications.* IEEE Access, 2024.
6. Amiri, M., M. Salavati-Niasari, and A. Akbari, *Magnetic nanocarriers: evolution of spinel ferrites for medical applications.* Advances in colloid and interface science, 2019. **265**: p. 29-44.
7. Salih, S.J. and W.M. Mahmood, *Review on magnetic spinel ferrite (MFe2O4) nanoparticles: From synthesis to application.* Heliyon, 2023. **9**(6).
8. Gaffar, S., A. Kumar, and U. Riaz, *Synthesis techniques and advanced applications of spinel ferrites: A short review.* Journal of Electroceramics, 2023. **51**(4): p. 246-257.
9. Hao, A. and X. Ning, *Recent advances in spinel ferrite-based thin films: synthesis, performances, applications, and beyond.* Frontiers in Materials, 2021. **8**: p. 718869.
10. Gunjakar, J., et al., *Chemical synthesis of spinel nickel ferrite (NiFe2O4) nano-sheets.* Applied Surface Science, 2008. **254**(18): p. 5844-5848.
11. Morosanu, C.E., *Thin films by chemical vapour deposition*. Vol. 7. 2016: Elsevier.
12. Nesa, M., *Characterization of zinc-doped copper oxide thin films synthesized by spray pyrolysis technique.* 2016.
13. Chavan, A.R. et al., *Cu2+ substituted NiFe2O4 thin films via spray pyrolysis technique and their high-frequency devices application.* Journal of Alloys and Compounds, 2018. **769**: p. 1132-1145.
14. Magar, V.U., et al., *Structural and optical properties of nickel aluminate spinel ferrite thin films prepared by spray pyrolysis technique.* Journal of Materials Science: Materials in Electronics, 2024. **35**(14): p. 967.
15. Mechiakh, R., et al., *Correlation between microstructure and optical properties of nano-crystalline TiO2 thin films prepared by sol–gel dip coating.* Applied Surface Science, 2010. **257**(3): p. 670-676.
16. Gabal, M., et al., *Understanding the structural, magnetic, and electrical properties of MFe2O4 (M= Mg2+, Co2+, Ni2+, Cu2+, Zn2+) nanocrystalline ferrites. A comparative study.* Applied Physics A, 2025. **131**(2): p. 116.
17. Somvanshi, S.B., et al., *Influential diamagnetic magnesium (Mg2+) ion substitution in nano-spinel zinc ferrite (ZnFe2O4): thermal, structural, spectral, optical, and physisorption analysis.* Ceramics International, 2020. **46**(7): p. 8640-8650.
18. Chavan, G.N., et al., *Systematic investigation on synthesis, characterization, electrical, magnetic, and optical properties of Ni1-xCuxFe2O4 spinel ferrites.* Applied Physics A, 2025. **131**(12): p. 1008.

19. Rathod, S.V., et al., *Structural and optical characterization of Mg-doped nickel ferrite thin films.* Journal of Materials Science: Materials in Electronics, 2025. **36**(3): p. 191.
20. Shubhra, et al., *Impact of doping Gd3+ rare earth ion on structural, magnetic, and optical properties of cobalt and nickel ferrite nanomaterials.* Applied Physics A, 2021. **127**(11): p. 861.
21. Zhang, H., et al., *Fourier transform infrared characterization of nanometres.* Journal of Physics: Condensed Matter, 1998. **10**(48): p. 11121.